

A Hyperactive End to the Atlantic Hurricane Season

October–November 2020

Philip J. Klotzbach, Kimberly M. Wood, Michael M. Bell, Eric S. Blake,
Steven G. Bowen, Louis-Philippe Caron, Jennifer M. Collins, Ethan J. Gibney,
Carl J. Schreck III, and Ryan E. Truchelut

ABSTRACT: The active 2020 Atlantic hurricane season produced 30 named storms, 14 hurricanes, and 7 major hurricanes (category 3+ on the Saffir–Simpson hurricane wind scale). Though the season was active overall, the final two months (October–November) raised 2020 into the upper echelon of Atlantic hurricane activity for integrated metrics such as accumulated cyclone energy (ACE). This study focuses on October–November 2020, when 7 named storms, 6 hurricanes, and 5 major hurricanes formed and produced ACE of $74 \times 10^4 \text{ kt}^2$ ($1 \text{ kt} \approx 0.51 \text{ m s}^{-1}$). Since 1950, October–November 2020 ranks tied for third for named storms, first for hurricanes and major hurricanes, and second for ACE. Six named storms also underwent rapid intensification ($\geq 30 \text{ kt}$ intensification in $\leq 24 \text{ h}$) in October–November 2020—the most on record. This manuscript includes a climatological analysis of October–November tropical cyclones (TCs) and their primary formation regions. In 2020, anomalously low wind shear in the western Caribbean and Gulf of Mexico, likely driven by a moderate-intensity La Niña event and anomalously high sea surface temperatures (SSTs) in the Caribbean, provided dynamic and thermodynamic conditions that were much more conducive than normal for late-season TC formation and rapid intensification. This study also highlights October–November 2020 landfalls, including Hurricanes Delta and Zeta in Louisiana and in Mexico and Hurricanes Eta and Iota in Nicaragua. The active late season in the Caribbean would have been anticipated by a statistical model using the July–September-averaged ENSO longitude index and Atlantic warm pool SSTs as predictors.

KEYWORDS: Atlantic Ocean; Tropics; ENSO; Hurricanes/typhoons; Tropical cyclones

<https://doi.org/10.1175/BAMS-D-20-0312.1>

Corresponding author: Philip J. Klotzbach, philk@atmos.colostate.edu

In final form 12 June 2021

©2022 American Meteorological Society

For information regarding reuse of this content and general copyright information, consult the [AMS Copyright Policy](#).

AFFILIATIONS: **Klotzbach** and **Bell**—Department of Atmospheric Science, Colorado State University, Fort Collins, Colorado; **Wood**—Department of Geosciences, Mississippi State University, Mississippi State, Mississippi; **Blake**—National Hurricane Center, National Oceanic and Atmospheric Administration, Miami, Florida; **Bowen**—Aon, Chicago, Illinois; **Caron**—Ouranos, Montreal, Quebec, Canada, and Barcelona Supercomputing Center, Barcelona, Spain; **Collins**—School of Geosciences, University of South Florida, Tampa, Florida; **Gibney**—UCAR/Cooperative Programs for the Advancement of Earth System Science, San Diego, California; **Schreck**—North Carolina Institute for Climate Studies, Cooperative Institute for Satellite Earth System Studies, North Carolina State University, Asheville, North Carolina; **Truchelut**—WeatherTiger, LLC, Tallahassee, Florida

* Klotzbach and Wood contributed equally to this work.

The 2020 Atlantic hurricane season was very active by most tropical cyclone (TC) metrics, producing a total of 30 named storms, 14 hurricanes, and 7 major hurricanes [maximum sustained winds ≥ 96 kt ($1\text{ kt} \approx 0.51\text{ m s}^{-1}$); categories 3–5 on the Saffir–Simpson hurricane wind scale]. The formation of 30 named storms broke the Atlantic single-season record of 28 named storms set in 2005, and only 2005 produced more hurricanes with a total of 15 (Beven et al. 2008). Seven major hurricanes formed in 2020, tying 2005 for the most major hurricanes on record dating back to 1851 (Landsea and Franklin 2013). Though the 2020 Atlantic hurricane season was on record pace for named storm formations through September (Table 1), the extremely active October–November (Oct–Nov) drove integrated metrics such as named storm days, major hurricane days, and accumulated cyclone energy¹ (ACE; Bell et al. 2000) to well above-average levels by the end of the season. Through 30 September, the 2020 Atlantic hurricane season produced 23 named storms, 6 ahead of the prior record of 17 named storms set in 2005 and equaled in 2011. However, during this time period the Atlantic only generated 19 hurricane days, just above the 1950–2019 average of 18.75 hurricane days. Also, total ACE reached $106 \times 10^4\text{ kt}^2$ by 30 September (~130% of the 1950–2019 average).

October–November 2020 was extremely active with 7 named storms, 6 hurricanes, and 5 major hurricanes forming during the 2-month period (Table 1). In addition, these two months generated $74 \times 10^4\text{ kt}^2$ of ACE, producing the second-most Oct–Nov ACE since 1950 (trailing only 2016 which produced $79 \times 10^4\text{ kt}^2$ of ACE). The 1950–2019 Oct–Nov average is 2.7 named storms, 1.5 hurricanes, 0.5 major hurricanes, and $23 \times 10^4\text{ kt}^2$ of ACE. The five major hurricanes that formed in Oct–Nov 2020 (Delta, Epsilon, Zeta, Eta, and Iota) were the most on record for the Atlantic basin during this 2-month period. No other season on record had more than two major hurricane formations in Oct–Nov. These two months in 2020 also generated five hurricane formations in the Caribbean Sea (Gamma, Delta, Zeta, Eta, and Iota), breaking the old record of three set in 1870 and equaled in 2010. All six Oct–Nov hurricanes hit land, causing extensive damage and loss of life (Table 2). Hurricane Gamma made landfall along the Yucatan Peninsula, and Delta and Zeta both made landfall in the Yucatan Peninsula and subsequently in Louisiana. Zeta's Yucatan landfall occurred near Gamma's landfall location a few weeks earlier. Hurricanes Eta and Iota made landfall at nearly the same location in Nicaragua as category 4 hurricanes less than two weeks apart, causing catastrophic damage, especially due to flooding and associated mudslides. Eta and Iota combined to cause \$7 billion USD in Honduras alone, which is ~30% of Honduras's gross domestic product of \$24 billion USD (Aon 2021). These storms

¹ Accumulated cyclone energy is an integrated metric accounting for frequency, intensity, and duration of storms and is calculated by squaring the maximum sustained wind speed at each 6-hourly interval when a tropical or subtropical cyclone has maximum sustained winds ≥ 34 kt (e.g., a named storm) and then dividing by 10,000.

Table 1. Observed Atlantic TC statistics for the 2020 Atlantic hurricane season through September, for October–November 2020, and for the full 2020 Atlantic hurricane season. Also included in parentheses are ranks for each TC statistic for each time period since 1950.

TC statistic	2020 Atlantic TC statistics through September	October–November 2020 TC statistics	Full 2020 Atlantic TC season statistics
Named storms	23 (1)	7 (T-3)	30 (1)
Named storm days	82.75 (4)	40 (2)	122.75 (2)
Hurricanes	8 (T-2)	6 (1)	14 (2)
Hurricane days	19 (32)	16.25 (4)	35.25 (17)
Major hurricanes	2 (T-21)	5 (1)	7 (T-1)
Major hurricane days	3.5 (T-34)	4.75 (4)	8.25 (20)
Accumulated cyclone energy	106 (18)	74 (2)	180 (8)

also combined to cause over 230 direct fatalities in Central America and southern Mexico, which thankfully was substantially fewer than the thousands of casualties resulting from Hurricane Mitch in 1998.

This manuscript examines the climatology of Oct–Nov Atlantic TCs, including its inter-annual variability as modulated by ENSO as well as its multidecadal variability that is likely modulated by the Atlantic multidecadal oscillation (AMO; Goldenberg et al. 2001; Klotzbach and Gray 2008; Klotzbach et al. 2018). We also discuss observed activity in Oct–Nov 2020 and then examine the large-scale drivers of the extremely active latter portion of the 2020 Atlantic hurricane season to compare against both the long-term climatology and 2005 specifically—another recent very active season in the Caribbean. Last, we examine the potential predictability of Oct–Nov Caribbean TC activity using a two-predictor model composed of the July–September-averaged ENSO longitude index (ELI; Williams and Patricola 2018) and July–September-averaged Atlantic warm pool (AWP; Wang and Lee 2007) conditions.

Table 2. October–November 2020 Atlantic named storm landfall summary statistics, including landfall location, intensity, estimated total damage and direct fatalities from individual NHC Tropical Cyclone Reports.

Storm name	Storm date (local time)	Landfall location	Landfall intensity (kt)	Landfall intensity (MSLP)	Estimated damage (millions USD)	Direct fatalities
Gamma	3 Oct 2020	Tulum, Mexico	65	978	Minimal	6
Delta	7 Oct 2020	Puerto Morelos, Mexico	90	971	185	0
Delta	9 Oct 2020	Creole, Louisiana	85	970	2,900	2
Zeta	26 Oct 2020	Tulum, Mexico	75	977	Minimal	0
Zeta	28 Oct 2020	Cocodrie, Louisiana	100	970	4,400	5
Eta	3 Nov 2020	Puerto Cabezas, Nicaragua	120	940	6,800	165
Eta	8 Nov 2020	Sancti Spiritus, Cuba	55	991	Minimal	0
Eta	9 Nov 2020	Lower Matecumbe Key, Florida	55	993	1,500	7
Eta	12 Nov 2020	Cedar Key, Florida	45	996	Combined with prior FL landfall	Combined with prior FL landfall
Iota	16 Nov 2020	Puerto Cabezas, Nicaragua	125	921	1,400	67

Data and significance tests

Atlantic TC dataset. All TC metrics are computed from the National Hurricane Center’s Atlantic hurricane database (HURDAT2; Landsea and Franklin 2013). This dataset currently provides 6-hourly location and intensity information for all TCs from 1851 to 2020. Though the Atlantic hurricane database is generally more reliable since the start of the Atlantic geostationary satellite era (since 1966; Landsea 2007), we extend our TC analysis back to 1950 given that the preponderance of Oct–Nov hurricane activity occurred in the better-observed western Atlantic. Western Atlantic TCs are more likely to have been observed by ships or aircraft reconnaissance compared to Atlantic TCs farther east. In addition, in the next section we show that Oct–Nov TC activity was more intense during the 1950s and 1960s than in the 1970s and 1980s, and consequently this backward extension of the TC dataset increases the sample size for our climatological analysis.

Reanalysis dataset. We use the European Centre for Medium-Range Weather Forecasts (ECMWF) fifth generation reanalysis dataset (ERA5; Hersbach et al. 2020) for all large-scale atmospheric and oceanic parameter calculations. The reanalysis is available at 0.25° spatial resolution and hourly temporal resolution. The ERA5 dataset extends from 1979 to near present. A preliminary backward extension of ERA5 to 1950 has recently been released, but we focus our large-scale analysis from 1979 onward, as this is the era of global geostationary and polar-orbiting satellite coverage (Smith et al. 1979).

Relative humidity and SST are directly provided by ERA5. Vertical wind shear is calculated as the vector wind difference between 200 and 850 hPa. Velocity potential anomalies are computed from 200-hPa vector winds using “windspharm” (Dawson 2016). Potential intensity is computed via “pyPI” (Gilford 2020), which uses the Bister and Emanuel (2002) algorithm.

ENSO dataset. We use the ELI (Williams and Patricola 2018) to define ENSO events. The ELI is calculated by averaging the longitude across the equatorial Pacific where the SST threshold for deep convection is met, a threshold defined as the SST averaged over the region from 5°S to 5°N . Williams and Patricola (2018) showed that the ELI has a stronger physical tie to the Walker circulation and exhibits stronger correlations with seasonal Atlantic hurricane activity than the oceanic Niño index, which is defined as a 3-month running average of SST anomalies in the Niño-3.4 region (5°S – 5°N , 170° – 120°W ; Barnston et al. 1997) (figure not shown). The physical basis for this stronger relationship is likely through shifts in the Walker circulation impacting vertical wind shear, which is one of the primary mechanisms by which ENSO significantly impacts Atlantic hurricane activity (Gray 1984).

Madden–Julian oscillation index. The Madden–Julian oscillation (MJO; Madden and Julian 1971) is the leading intraseasonal mode of variability in tropical convection. The MJO typically propagates around the globe every 30–70 days. The phase and amplitude of the MJO can be quantified by the Wheeler–Hendon (WH) index (Wheeler and Hendon 2004). The WH index uses 200- and 850-hPa zonal wind along with outgoing longwave radiation to determine the location and intensity of the rising branch of the MJO. The MJO has been shown to significantly modulate Atlantic hurricane activity on intraseasonal time scales via modulations in vertical wind shear, midlevel moisture, and vertical motion over the tropical Atlantic and Caribbean (Klotzbach 2010; Ventrice et al. 2011; Klotzbach and Oliver 2015).

Statistical significance tests. Statistical significance is calculated using bootstrap resampling methods (Efron 1979; Wilks 1997; Hesterberg et al. 2003). Statistical significance of differences in means and statistical significance of correlations are calculated by resampling randomly from the specific dataset(s) being investigated with replacement 1,000 times. If the

mean obtained in our sample occurs fewer than 5% of the time in the randomly resampled dataset, the mean is considered statistically significant, while if fewer than 5% of the randomly resampled correlations are of the opposite sign of the correlation obtained in the analysis, the correlation is said to be significant at the 5% level.

October–November Atlantic tropical cyclone climatology

Interannual and multidecadal variability. October and November are the final two months of the official Atlantic hurricane season, which runs from 1 June to 30 November. Using a 1950–2019 climatology, an average Oct–Nov (33% of the season length) generates 22% of named storm formations, 24% of hurricane formations, 20% of major hurricane formations, and 22% of ACE (Fig. 1). In this manuscript, formation refers to when a TC first reaches a particular intensity. For example, if a TC became a named storm on 30 September and a hurricane on 3 October, it would count as a September named storm and an October hurricane. We leave 2020 out of most of the climatological discussion that follows to compare the 2020 season against a climatology that does not include the season on which this paper focuses.

There is pronounced interannual and multidecadal variability in Oct–Nov Atlantic hurricane activity from 1950 to 2019 (Fig. 2). Here, we focus on ACE to highlight this variability. In 1960, 1983, and 1993, the final two months of the Atlantic hurricane season generated 0 ACE, while 2016 produced the most Oct–Nov ACE since 1950 ($79 \times 10^4 \text{ kt}^2$). October–November 2020 (red bar in Fig. 2a) generated the second-most ACE during the 2-month period ($74 \times 10^4 \text{ kt}^2$). Figure 2a also highlights pronounced multidecadal variability in Oct–Nov Atlantic hurricane activity, with heightened activity from 1950 to 1969 and 1995 to 2019 but less activity from 1970 to 1994. These multidecadal periods have been associated with the AMO, with 1950–69 and 1995–present regarded as positive AMO phases and 1970–94 regarded as a negative AMO phase. Positive AMO phases are typically characterized by higher tropical Atlantic SSTs and reduced vertical wind shear, both of which favor more Atlantic hurricane activity (Goldenberg et al. 2001; Klotzbach and Gray 2008). The average ACE observed from 1950 to 1969 ($28 \times 10^4 \text{ kt}^2$) and from 1995 to 2019 ($29 \times 10^4 \text{ kt}^2$) are significantly higher than the average ACE observed from 1970 to 1994 ($12 \times 10^4 \text{ kt}^2$).

As is the case for overall seasonal TC activity (Gray 1984; Tang and Neelin 2004; Klotzbach 2007), ENSO strongly modulates Oct–Nov Atlantic TC activity (Figs. 2a,b). The dashed line in the scatterplot of the ELI and Oct–Nov ACE time series (Fig. 2b) highlights the linear regression between the two time

series. A more westward ELI index (e.g., a westward-shifted Walker circulation) is typically associated with lower SSTs in the eastern and central tropical Pacific (e.g., La Niña) and higher levels of Atlantic ACE. Though the strength of the relationship is fairly weak (e.g., $r = -0.31$ from 1950 to 2019), the correlation is statistically significant. We also stratify ENSO by dividing 1950–2019 ELI values into three bins (selecting the 17 most eastward ELI values for El Niño, the 17 most westward ELI values for La Niña, and the middle 36 ELI values for ENSO neutral) and compute the mean of the observed ACE values in each subset. The mean Oct–Nov ACE for El Niño years is $14 \times 10^4 \text{ kt}^2$, the mean Oct–Nov ACE for ENSO neutral years

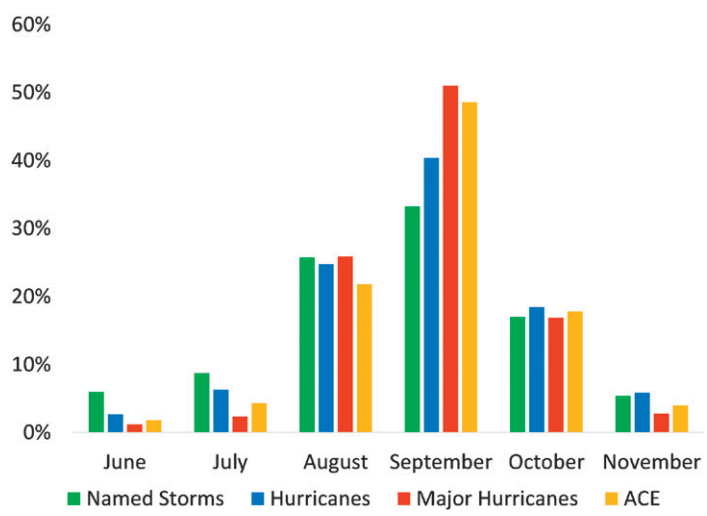


Fig. 1. Percentage of Atlantic tropical cyclone activity generated in each month of the Atlantic hurricane season using a 1950–2019 climatology.

is $23 \times 10^4 \text{ kt}^2$, and the mean Oct–Nov ACE for La Niña years is $31 \times 10^4 \text{ kt}^2$. Both the average El Niño and the average La Niña ACE are significantly different from ENSO-neutral ACE. In addition, only two of the 17 El Niño years had ACE greater than $30 \times 10^4 \text{ kt}^2$, while eight of the 17 La Niña years had ACE greater than $30 \times 10^4 \text{ kt}^2$. We do also note that there is a large spread in observed ACE in La Niña and ENSO-neutral years, indicating that other large-scale conditions besides ENSO play an important role in modulating late season Atlantic hurricane activity. The red dot denotes the observed ACE and ELI for Oct–Nov 2020. The Oct–Nov ELI in 2020 was the seventh-farthest west since 1950, indicative of a La Niña event.

October–November Atlantic TC formation locations and track characteristics.

Figure 3a displays October Atlantic named storm formations from 1950 to 2019. The dot plotted on each map represents the location where each named storm first reached tropical storm strength (e.g., $\geq 34\text{-kt}$ maximum sustained winds), with warmer colors indicating stronger maximum intensities. Named storm formations occur throughout the basin, yet of the 20 October named storms that reached major hurricane strength, 14 (70%) formed in the Caribbean. In addition, of the 75 October named storms that reached hurricane strength, 53 (71%) formed in the western Atlantic (west of 60°W). As would be expected given where named storms form during October, most October major hurricane tracks also occurred in the Caribbean (Fig. 3c). This ratio contrasts with September Atlantic named storm formations, where 41% of named storms that reached hurricane strength formed in the western Atlantic. DeMaria et al. (2001) highlighted that tropical Atlantic named storm formations between Africa and the Caribbean (e.g., south of 20°N , east of 60°W) typically decrease by early October due to increasing vertical wind shear.

Five November major hurricanes formed during 1950–2019, with all but Hurricane Kate (1985) occurring in the western Caribbean (Fig. 3b). The central subtropical Atlantic also produces frequent November Atlantic named storm formations, typically of the baroclinically initiated variety (e.g., Elsner et al. 1996; McTaggart-Cowan et al. 2013; Tang et al. 2020). All November named storms that became major hurricanes have had relatively short lifespans at major hurricane strength (Fig. 3d), given that most of these major hurricanes have formed

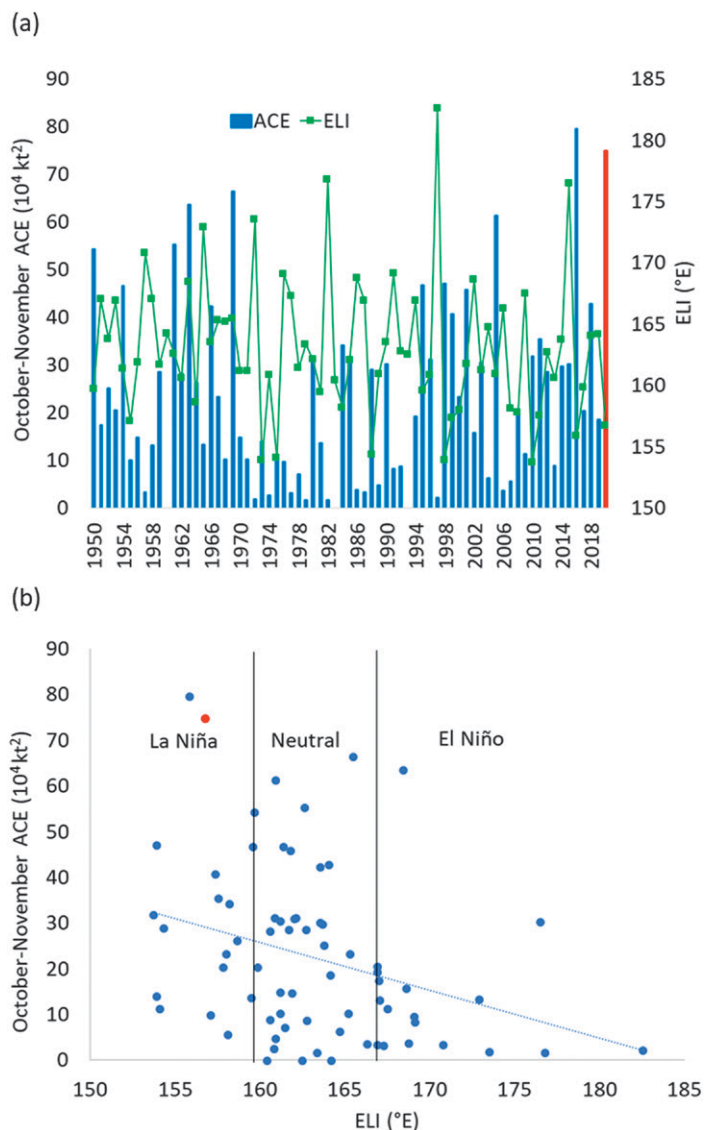


Fig. 2. (a) October–November Atlantic ACE from 1950 to 2020 (blue columns) and the ENSO longitude index (ELI) (green line). The red column highlights the observed ACE in October–November 2020. (b) Scatterplot of the relationship between October–November ACE and ENSO from 1950 to 2020 as represented by the ELI. The red dot represents the observed value of the ELI and October–November ACE in 2020, while the blue dashed line represents the regression relationship between the two time series from 1950 to 2019. Black lines delineate the longitude breakdowns between El Niño and neutral and neutral and La Niña conditions, respectively.

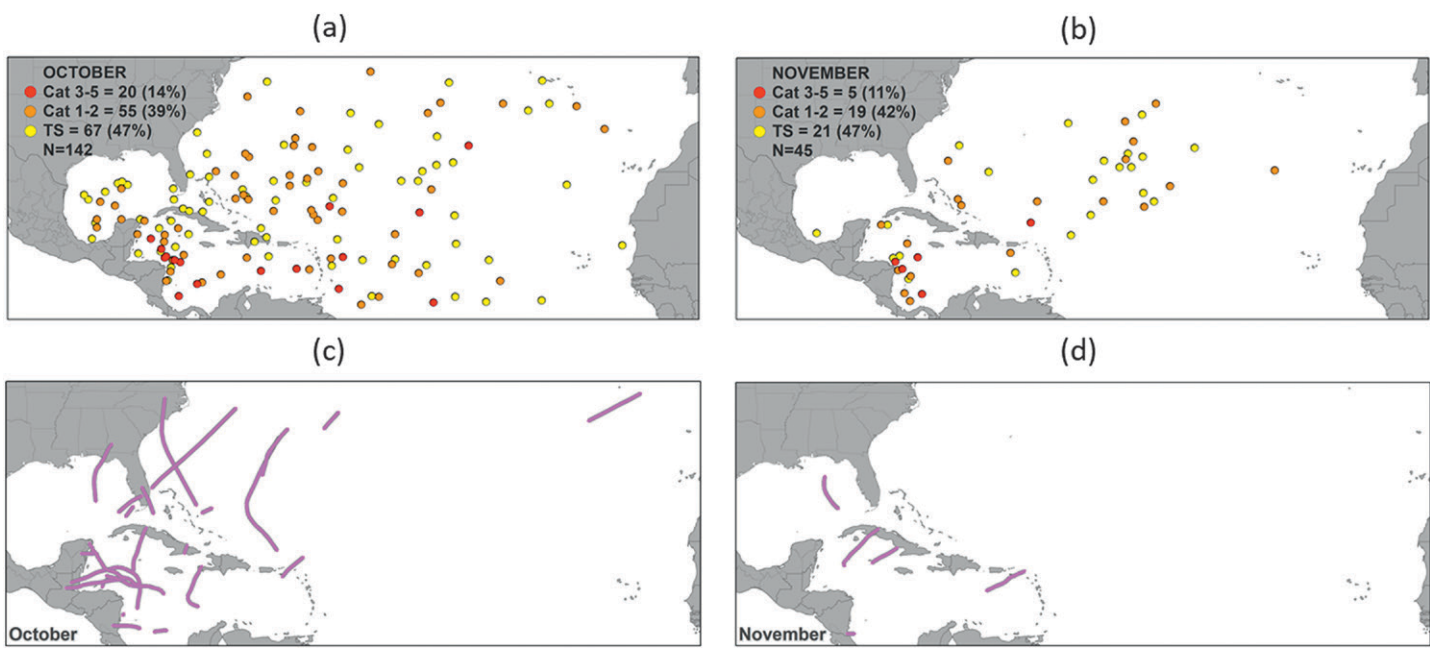


Fig. 3. (a) October Atlantic named storm formation locations from 1950 to 2019. Named storms that reached major hurricane strength are denoted by red dots, category 1–2 hurricane strength are denoted by orange dots, and tropical storm strength are denoted by yellow dots. (b) As in (a), but for November Atlantic named storm formation locations. (c) October Atlantic tropical cyclone tracks at major hurricane strength from 1950 to 2019. (d) As in (c), but for November major hurricane-strength tracks.

in the western Caribbean and consequently close to land. All five November major hurricanes between 1950 and 2019 made landfall and caused considerable damage: Kate in 1985 (Case 1985), Lenny in 1999 (Guiney 1999), Michelle in 2001 (Beven 2002), Paloma in 2008 (Brennan 2009), and Otto in 2016 (Brown 2017).

October–November 2020 Atlantic tropical cyclone activity

October named storm activity. As noted in the introduction, Oct–Nov 2020 was extremely prolific for Atlantic TC activity, with 7 named storms, 6 hurricanes, and 5 major hurricanes occurring during the 2-month period (Table 1 and Figs. 4a,c). Following an extremely active period for Atlantic TC activity during mid-September that featured three hurricanes simultaneously (Paulette, Sally, and Teddy), the Atlantic went through a lull with no named storm activity from 23 September through 1 October. However, that lull ended when Gamma became a named storm on 2 October in the western Caribbean and intensified to a 65-kt hurricane before making landfall along the Yucatan Peninsula (Latto 2021). Though Gamma caused minimal damage in Mexico, 6 direct fatalities in Mexico were attributed to the storm.

On 5 October, Delta formed in the central Caribbean and rapidly intensified to a category 4 hurricane on 6 October, peaking at 120-kt maximum sustained winds before weakening and making landfall on the Yucatan Peninsula (Cangialosi and Berg 2021). Delta reintensified in the Gulf of Mexico to category 3 intensity but then weakened to an 85-kt hurricane before making landfall near Cameron, Louisiana, on 9 October. Delta's Mexico landfall caused an estimated \$185 million USD in damage, while its landfall in Louisiana caused \$2.9 billion USD in damage. Delta did not cause any direct fatalities in Mexico but did cause five direct fatalities in the southeastern United States.

After another brief lull in TC activity in mid-October, Epsilon formed in the subtropical central Atlantic from a nontropical low on 19 October (Papin 2021). It underwent rapid intensification between 20 and 21 October and reached 100-kt major hurricane intensity while east of Bermuda. Epsilon became a major hurricane at 29.3°N—the farthest north an

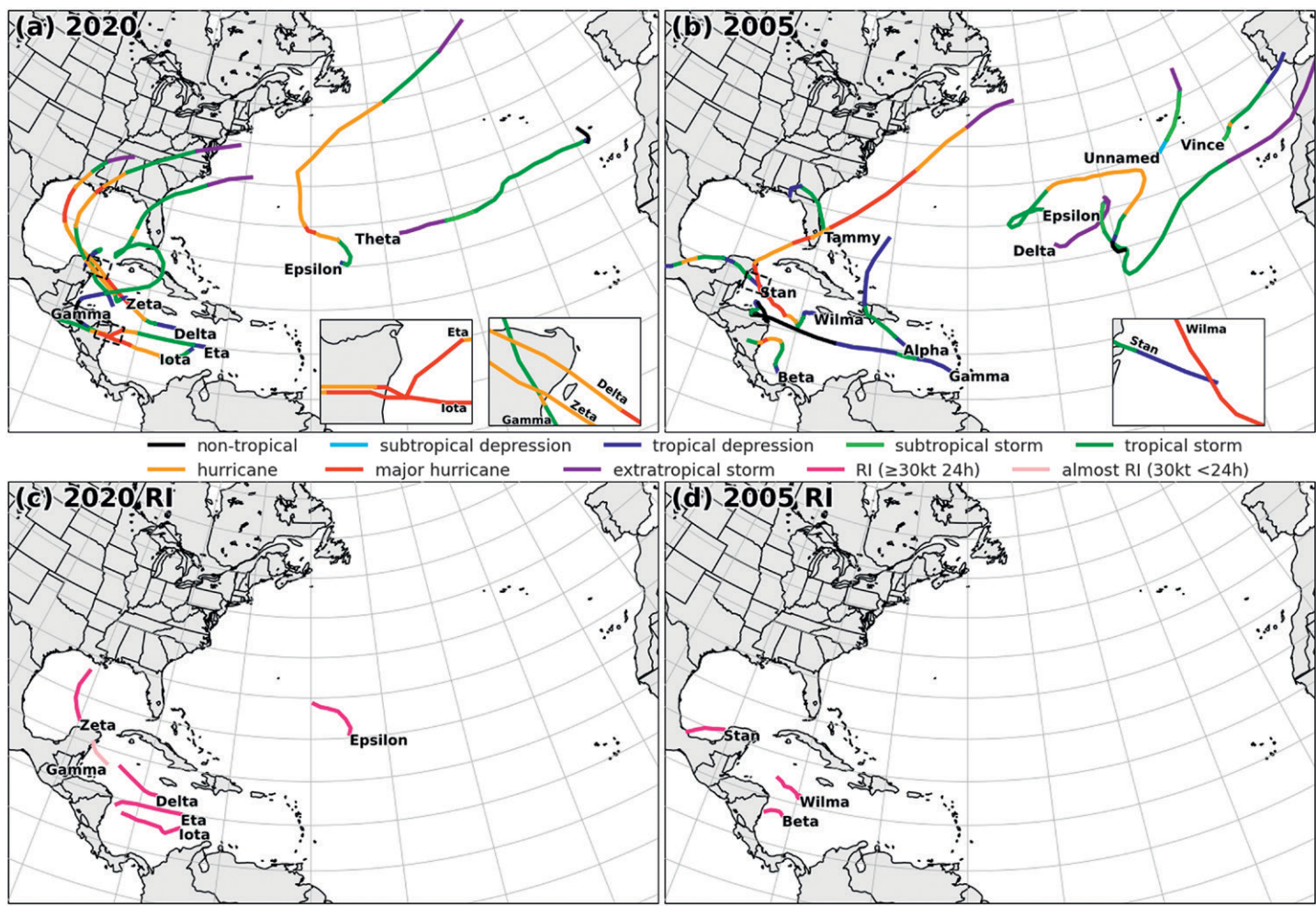


Fig. 4. (a) Tracks of Atlantic tropical cyclones in Oct–Nov 2020. (b) As in (a), but for Oct–Nov 2005. (c) Tracks of named storms during their rapid intensification stage in Oct–Nov 2020. (d) As in (c), but for Oct–Nov 2005.

Atlantic major hurricane has formed this late in the calendar year (21 October) on record. While Epsilon caused only minor damage, one direct fatality was recorded in Florida due to rip currents generated by the storm.

Zeta was named on 25 October while in the northwest Caribbean Sea (Blake et al. 2021). It was initially slow to intensify but then strengthened more rapidly, reaching hurricane strength by 26 October before making landfall on the Yucatan Peninsula on 27 October. Zeta weakened to a tropical storm after landfall but then rapidly intensified after reaching the Gulf of Mexico, peaking at 100 kt (e.g., major hurricane intensity) before making landfall in southeast Louisiana on 28 October. Zeta's Mexican landfall caused only minimal damage and no direct fatalities, while Zeta's landfall in Louisiana caused \$4.4 billion USD in damage and five direct fatalities.

November named storm activity. Eta was named in the central Caribbean on 1 November and, after an initial steady intensification, began rapidly intensifying on 2 November, reaching a peak intensity of 130 kt early on 3 November (Pasch et al. 2021). Eta weakened slightly to 120 kt before making landfall in Nicaragua later that day. The system continued to weaken to a tropical storm on 4 November and then to a tropical depression on 5 November. However, after weakening to a tropical disturbance while moving over the mountainous terrain of Nicaragua and then Honduras, Eta intensified into a tropical depression on 6 November once it reemerged over the northwest Caribbean. It slowly became better organized, reintensifying to a tropical storm before making landfall at 55 kt in south-central Cuba on 8 November. Eta then tracked

northeastward and then northwestward, making another landfall on 9 November in the Florida Keys as a 55-kt tropical storm. It then weakened slightly while moving southwestward over the southern Gulf of Mexico. Eta subsequently turned northeastward and underwent one last burst of intensification, briefly reaching hurricane strength on 11 November before dry air and shear began to weaken the system. It made a final landfall near Cedar Key, Florida, on 12 November as a 45-kt tropical storm. Eta caused \$6.8 billion USD in damage and 165 direct fatalities in Central America and southern Mexico and also caused \$1.5 billion USD in damage and 7 direct fatalities in the United States.

Theta formed from a nontropical area of low pressure on 10 November in the subtropical central Atlantic (Beven 2021). It was initially classified as subtropical but became a tropical storm later that day. Theta also reached its maximum intensity of 60 kt on 10 November. No damage or casualties were attributed to Theta.

Iota became a named storm in the central Caribbean on 13 November (Stewart 2021). Some westerly shear and dry air entrainment slowed Iota's initial intensification, but it then underwent rapid intensification from 45 kt late on 14 November to its peak intensity of 135 kt on 16 November. Iota weakened slightly before making landfall in Nicaragua on 17 November as a 125-kt hurricane ~25 km south of where Eta made landfall just 13 days prior. Iota caused \$1.4 billion USD in damage and was responsible for 67 direct fatalities in Central and South America.

October–November 2020 landfalls and rapidly intensifying hurricanes. The 2020 Atlantic hurricane season ranked in the top five (since 1950) for all Oct–Nov Atlantic TC statistics analyzed here (Table 1). Overall activity levels were high, yet what made Oct–Nov 2020 even more notable was the sheer number and intensity of its landfalls (Fig. 4a). Five of the seven named storms that formed made at least one landfall, with Eta making four separate landfalls. Eta and Iota made landfall in nearly the same location in Nicaragua thirteen days apart, causing tremendous damage and devastation to Nicaragua, Honduras, and other parts of Central America. Also, Gamma, Delta, and Zeta made landfall at nearly the same spot along the Yucatan Peninsula. Delta and Zeta made landfall in Louisiana as category 2 and category 3 hurricanes, respectively, bringing additional significant damage to a state that had already been hit by Hurricane Laura just several weeks prior. The financial toll from Eta and Iota across Central America was heavily driven by excessive rainfall that prompted considerable flooding and landslides. This part of the world is highly conducive to flooding given the local topography. The combined damage of these storms was comparable to Hurricane Mitch (1998), which caused ~\$6 billion (2020 USD) in damage in Central America (EM-DAT 2021). However, Eta and Iota's estimated direct fatality loss of ~230 paled in comparison to that of Hurricane Mitch's estimated 9,000 fatalities (Pasch et al. 2001), likely due to improved warning capabilities in those countries in recent years.

One of the other notable features of Oct–Nov 2020 was the prevalence of rapidly intensifying named storms (Fig. 4c). A threshold of 30 kt in 24 h has been applied to define rapid intensification in prior studies, as it represents approximately the 95th percentile of 24-h overwater intensity change in the Atlantic basin (e.g., Kaplan and DeMaria 2003; Kaplan et al. 2010). Here we use this same criterion for named storms that were at least tropical-storm strength at the start of their rapid intensification event, as tropical depression classifications have less certainty going back in time (Klotzbach and Landsea 2015). We also include Gamma as a rapidly intensifying storm, as it intensified by 30 kt in less than 24 h but then weakened due to landfall. Six of the seven named storms that formed in Oct–Nov 2020 underwent rapid intensification (Gamma, Delta, Epsilon, Zeta, Eta, and Iota). These six Oct–Nov named storms undergoing rapid intensification are the most on record for the Atlantic basin during Oct–Nov, breaking the old record of three rapidly intensifying named storms set in 2005 (Fig. 4d) and

equaled in 2010. However, more noteworthy was that three named storms in Oct–Nov 2020 had rapid intensification episodes ≥ 65 kt in 24 h (Delta, Eta, and Iota). Prior to 2020, only one named storm (since 1950) had intensified by more than 60 kt in 24 h in Oct–Nov. Wilma (2005) set the 24-h Atlantic named storm rapid intensification record when it intensified by 95 kt in 24 h. Extremely favorable large-scale conditions in 2020, as discussed in the next section, provided an environment that was highly conducive for rapid intensification to occur.

Comparison with October–November 2005. As noted in the introduction, Oct–Nov 2005 was also very active, with 10 named storms, 4 hurricanes, 2 major hurricanes, and 61×10^4 kt² of ACE (Fig. 4b). Though more named storms occurred in Oct–Nov 2005 than Oct–Nov 2020, Oct–Nov 2020 produced more hurricanes, major hurricanes, and ACE. The Oct–Nov portion of the 2005 season was also impactful from a landfall perspective, with three named storms making landfall at hurricane strength: Stan, Wilma, and Beta. Wilma's landfall on the Yucatan Peninsula with 130-kt maximum sustained winds was the strongest Oct–Nov landfall in 2005. Wilma would then go on to make a second landfall in southwest Florida with 105-kt maximum sustained winds, causing considerable damage across the southern part of the state. Torrential rainfall associated with Stan, and a larger Central American gyre (Papin et al. 2017) in which Stan was embedded, resulted in more than 1,000 fatalities in Central America (Pasch and Roberts 2006). Total damage from landfalling named storms in Oct–Nov 2005 was \$41 billion (2020 USD), primarily from Wilma and Stan (EM-DAT 2021).

Prior to landfall, Stan, Wilma, and Beta all underwent rapid intensification in Oct–Nov 2005. Wilma intensified by 95 kt in 24 h, the greatest 24-h intensification rate ever recorded in the Atlantic. Both Stan and Beta intensified by 30 kt in 24 h, and as noted earlier, three of the Oct–Nov 2020 hurricanes intensified by ≥ 65 kt in 24 h: Delta, Eta, and Iota. The environmental parameter analysis in the next section discusses which large-scale atmospheric and oceanic conditions likely led to extreme activity in both Oct–Nov 2005 and Oct–Nov 2020.

October–November 2020 Atlantic basin large-scale analysis

We now evaluate ERA5 monthly averaged fields to place Oct–Nov 2020 in the context of past seasons with additional comparison against Oct–Nov 2005. To explore subregional conditions within the Atlantic basin, we define the western Caribbean as 10°–20°N, 84°–72°W; the eastern Caribbean as 10°–20°N, 72°–60°W; and the Gulf of Mexico as 20°–30°N, 97°–81°W (indicated by dashed boxes in Fig. 5d). Only three Oct–Nov hurricanes have formed in the tropical Atlantic (south of 20°N, east of 60°W) since 1950, likely due to climatological increases in vertical wind shear (DeMaria et al. 2001), thus we focus on the aforementioned three subregions in the discussion that follows.

In October 2020, high SST and moisture coincided with low vertical wind shear in the western Caribbean and southwestern Gulf of Mexico (Fig. 5), where Gamma, Delta, and Zeta developed and tracked (Fig. 4a). Potential intensity was also high in that area (Fig. 5b), indicating environmental conditions that were generally conducive for stronger TCs. We do note that regions with hatched potential intensity (indicating top five most favorable) were generally smaller than regions with favorable SST in both October (Figs. 5a,b) and November 2020 (Figs. 6a,b). As was shown by Johnson and Xie (2010), the threshold for tropical convection increases in a warming climate, and consequently, a measure of tropospheric stability such as potential intensity may be a better indicator than SST of how anthropogenic climate change may impact TC activity over time.

By comparison, although the eastern Caribbean also had elevated moisture, it also tended to have higher shear, particularly east of 70°W (Figs. 5c,d). This shear pattern supported the observed spatial distribution of TC activity. No TCs developed south of 25°N and east of 72°W in October 2020 (Fig. 4a). However, wind shear was weaker in the southern part of the tropical

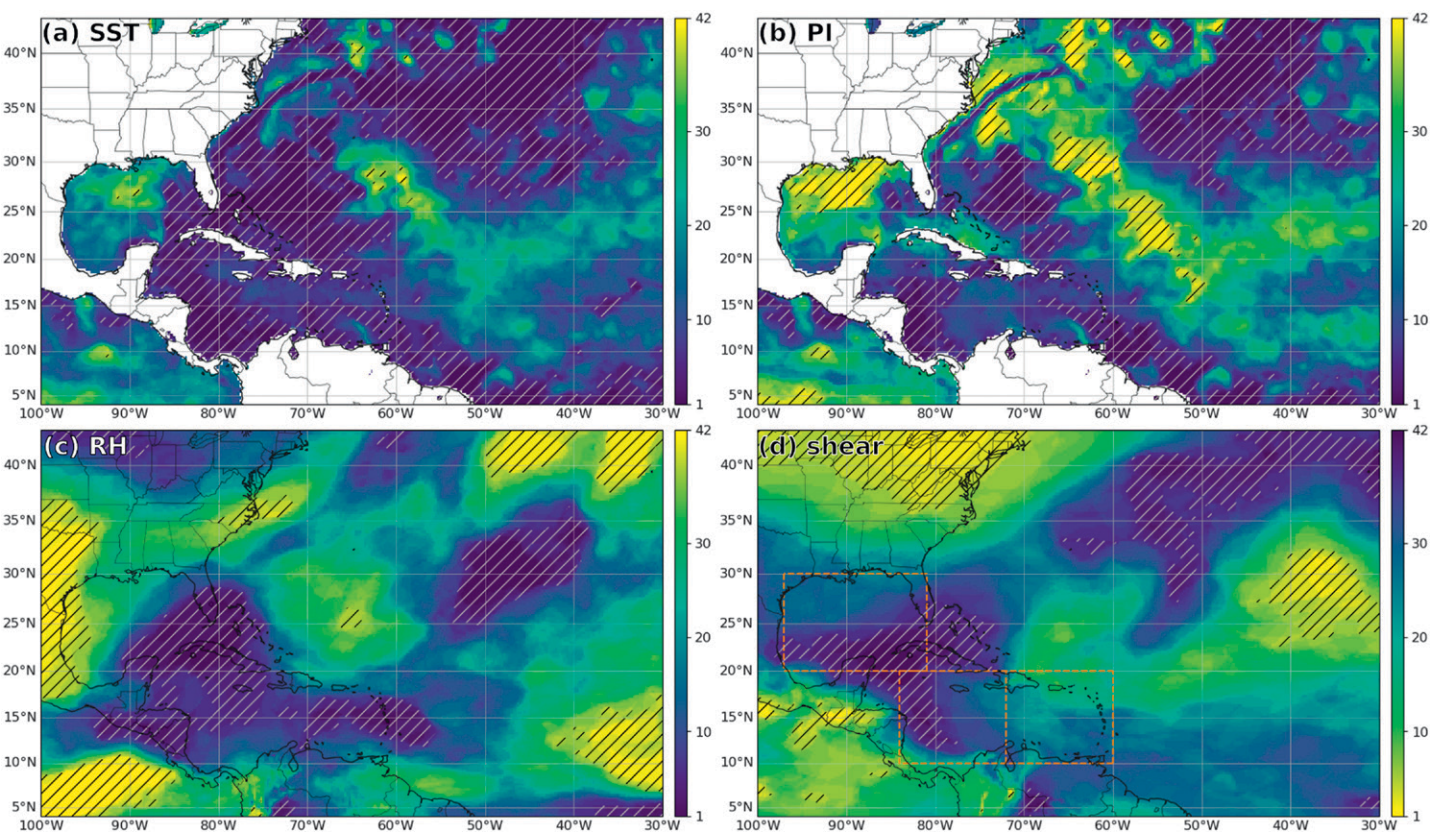


Fig. 5. Rank maps for October 2020 from ERA5 monthly averaged fields of (a) SST, (b) potential intensity, (c) 500–700-hPa relative humidity, and (d) 200–850-hPa wind shear. A rank of 1 represents the highest value during 1979–2020 and a rank of 42 the lowest. Purple shading indicates conditions more conducive for TCs; yellow shading indicates less conducive conditions. White hatching shows values that are in the top five most favorable for TCs, and black hatching shows values that are in the bottom five least favorable for TCs for each parameter. Orange dashed boxes in (d) represent the three geographic regions discussed in Fig. 7.

Atlantic (Fig. 5d), which may have allowed the African easterly waves that spawned Gamma, Delta, and Zeta to reach more favorable conditions in the Caribbean.

In November 2020, the western Caribbean was marked by extremely conducive conditions, with monthly averaged potential intensity, midlevel moisture, and shear ranking either the most or second-most conducive for the 1979–2020 period (Figs. 6, 7). These anomalously favorable conditions likely supported the explosive intensification observed for Hurricanes Eta and Iota. The Gulf of Mexico exhibited comparatively lower moisture and potential intensity, although climatologically TC activity in this region is relatively rare in November. Notably, all November major hurricanes since 1950—with the exception of Kate (1985)—formed and intensified in the Caribbean.

As noted earlier, October 2020 had lower vertical wind shear and more moist air in the western Caribbean and Gulf of Mexico compared with most other years (Figs. 5, 7a). We note that 2005 also had extremely favorable SST and potential intensity conditions in the Caribbean during October (Fig. 7b). Notably, two major hurricanes including the strongest Atlantic hurricane on record when measured by minimum sea level pressure (Wilma) formed in the Caribbean in October 2005.

During November 2020, the eastern Caribbean ranked highly for moisture and SST, while the western Caribbean ranked first or second for all but SST during the 42-year period (Fig. 7a). November 2005 exhibited environments generally less favorable than November 2020 across the three Atlantic regions defined earlier with few fields ranking in the top five years. In 2005, the western Caribbean had no November fields ranking in the top five years, and only

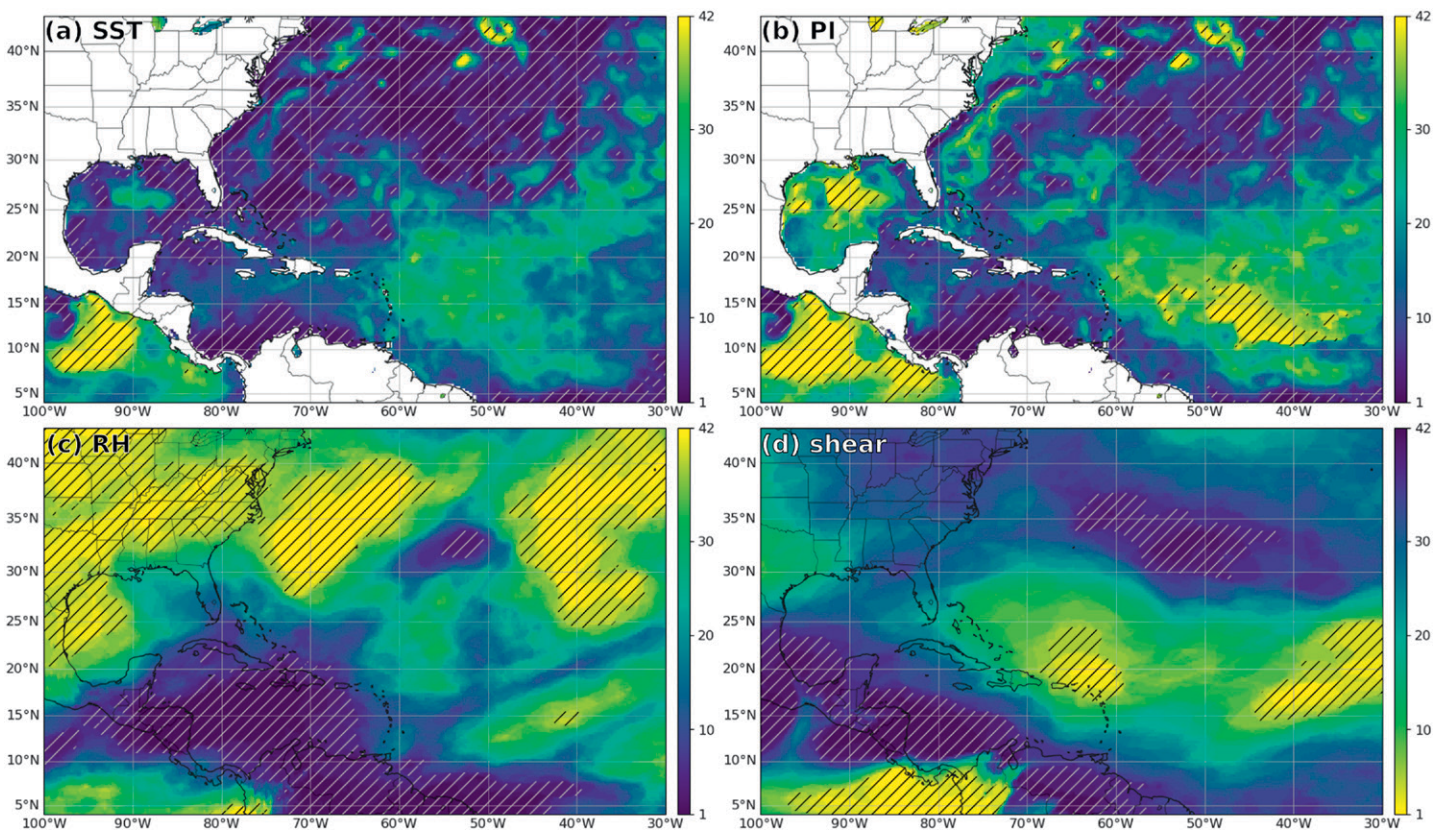


Fig. 6. As in Fig. 5, but for ERA5 monthly averaged fields in November 2020.

one weak named storm (Gamma) formed in the western Caribbean. Also in November 2005, Delta and Epsilon formed in the subtropics.

Given submonthly variability such as the unprecedented back-to-back major hurricanes in the Caribbean in November 2020 and the quiet periods in the Caribbean from mid-to-late October and after mid-November, we now examine the role of subseasonal variability such as the MJO. Prior research has shown that when the MJO is enhancing convection over Africa and the western Indian Ocean (e.g., phases 1–2), Atlantic hurricane activity is enhanced, but when the MJO is enhancing convection over the tropical Pacific Ocean (e.g., phases 6–7), Atlantic hurricane activity is suppressed (Ventrice et al. 2011; Klotzbach and Oliver 2015).

The MJO index remained in phase 5 for most of October (Fig. 8a). We attribute this persistent MJO index value to a relatively stationary region of enhanced convection near the South China Sea ($\sim 120^{\circ}\text{E}$). This stationary pattern was associated with the intensifying La Niña circulation, but it was not yet being reflected in the 120-day running mean that is subtracted from the MJO index. While this stationary pattern was the primary subseasonal driver during October, there was also an eastward propagating signal. It can be seen most clearly in the convectively suppressed pattern near 90°W at the beginning of October that circumnavigates and returns to 90°W around the end of the month (Fig. 8b). Roundy (2012) found that the MJO and Kelvin waves exhibit a continuum of structures. This particular event lies closer to the MJO time scale on that continuum, but it was faster than most MJO events, as it propagated around the globe in ~ 30 days.

The propagating MJO signal likely enhanced conditions for the development of Gamma and Delta early in October, then the suppressed MJO phase and its associated increased vertical wind shear was likely associated with the relatively quiet period in late October. Eta and Iota formed when the propagating signal returned to the Western Hemisphere. By that time, the combined effects of the MJO and the stationary signals were transitioning into phases 8,

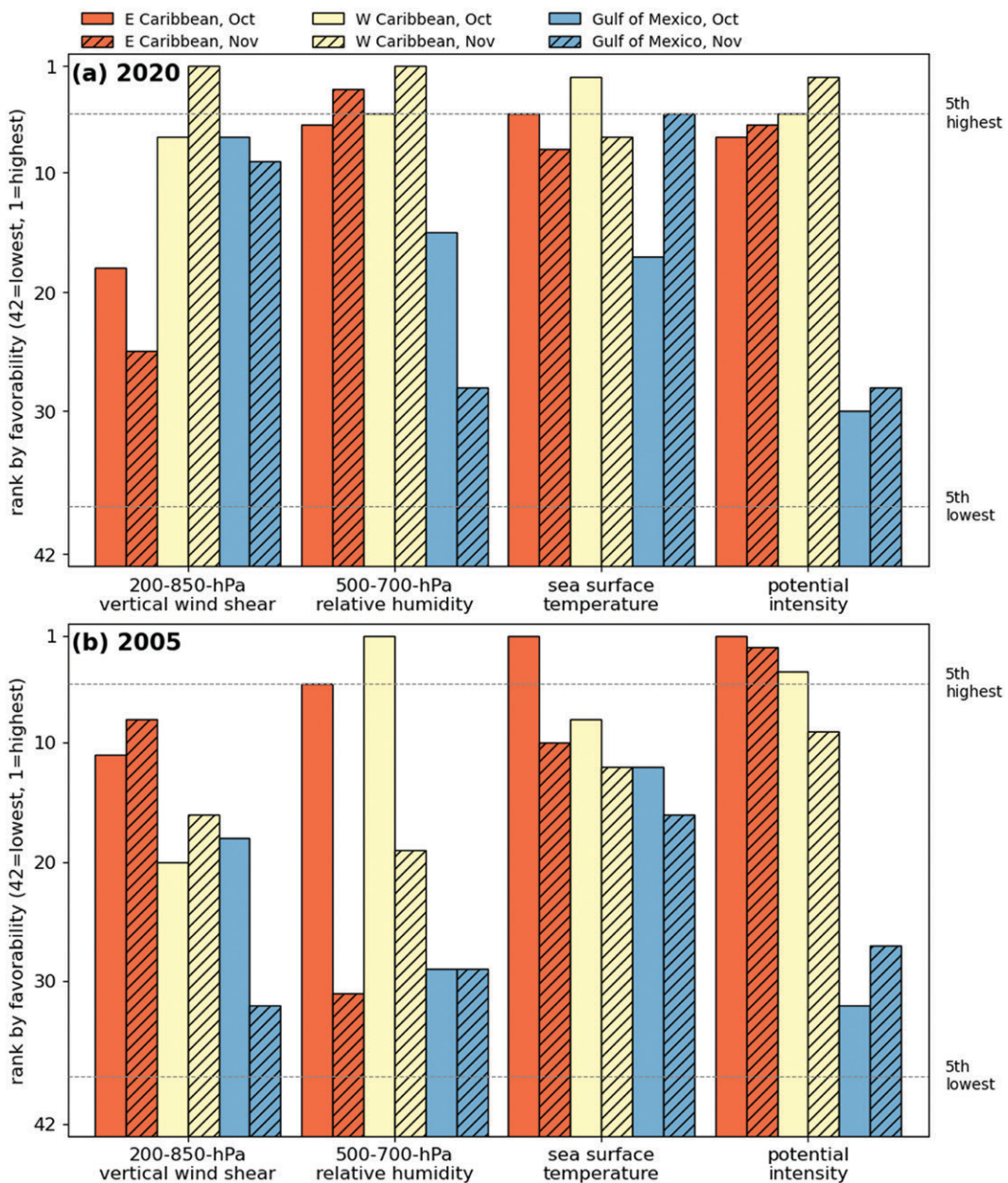


Fig. 7. October (solid) and November (hatched) monthly ranks of various fields by TC favorability within three Atlantic basin subregions (boxes in Fig. 5d) for (a) 2020 and (b) 2005. A rank of 1 indicates the most favorable during 1979–2020 (e.g., lowest wind shear, highest SST) and a rank of 42 indicates least favorable (e.g., highest wind shear, lowest SST).

1, and 2, which would have reduced vertical wind shear and favored Eta's persistence and Iota's development.

How well could we have anticipated October–November Caribbean hurricane activity in 2020?

Though there are no publicly available statistical models that forecast Oct–Nov Atlantic hurricane activity as a whole, Klotzbach (2011) developed a two-predictor model using ENSO and the AWP (Wang and Lee 2007) to hindcast Oct–Nov Caribbean hurricane days. That model used the July–September-averaged Niño-3.4 index as its ENSO parameter and July–September-averaged SSTs from 10°–20°N, 85°–50°W as its AWP parameter. In the analysis that follows, we replace the Niño-3.4 index with the ELI since we have used this index to define ENSO throughout this study. As in our prior SST analysis, we use ERA5 SST to calculate the

AWP predictor since 1979. Since this paper focuses on ACE, we hindcast Caribbean ACE as opposed to Caribbean hurricane days. Both parameters are linearly regressed against Caribbean ACE from 1979 to 2019, which Klotzbach (2011) defined as the region bounded by 10° – 20° N, 88° – 60° W. We use that same regional definition here. The July–September-averaged ELI predictor significantly correlates with Oct–Nov Caribbean ACE at -0.54, and the July–September-averaged AWP predictor significantly correlates with Oct–Nov Caribbean ACE at 0.52 (Figs. 9a,b).

We next develop a simple linear regression model for Oct–Nov Caribbean ACE using these two parameters as predictors. We rank observed ACE and rank hindcast ACE from the linear regression model and assign final ACE values to the hindcast model based on what the observed ACE would be given its rank. Since 16 years between 1979 and 2019 had 0 Oct–Nov Caribbean ACE, the 16 lowest ranked ACE hindcasts are also assigned a value of 0 ACE. The highest observed Oct–Nov Caribbean ACE occurred in 2016, when 35×10^4 kt² of ACE were generated. The model anticipated that 2010 would generate the most Oct–Nov Caribbean ACE during the hindcast period, and consequently, the hindcast for 2010 was assigned 2016’s observed value (e.g., 35×10^4 kt²). The correlation between observed Oct–Nov Caribbean ACE and hindcasts using the approach outlined in this section is 0.78, indicating that ~60% of the variance in Oct–Nov Caribbean ACE can be explained by this simple model (Fig. 9c). If we only consider the 25 years where the model hindcast nonzero ACE, the correlation between observed Oct–Nov Caribbean ACE and hindcast ACE remains quite high ($r = 0.75$). The model also shows robust skill at predicting ACE when only El Niño ($r = 0.87$), neutral ENSO ($r = 0.74$), and La Niña years are considered ($r = 0.64$).

Last, we apply this model to forecast Oct–Nov Caribbean ACE in 2020. July–September-averaged ELI was the seventh-farthest west on record (e.g., indicative of La Niña conditions), and the July–September averaged AWP was the fourth warmest on record. Since both predictors were favorable for Oct–Nov Caribbean ACE generation, the model predicted the fourth-most Oct–Nov Caribbean ACE since 1979 in 2020. The observed Oct–Nov 2020 Caribbean ACE was the 3rd highest on record (33×10^4 kt²). Operationally, we would have calculated the forecast

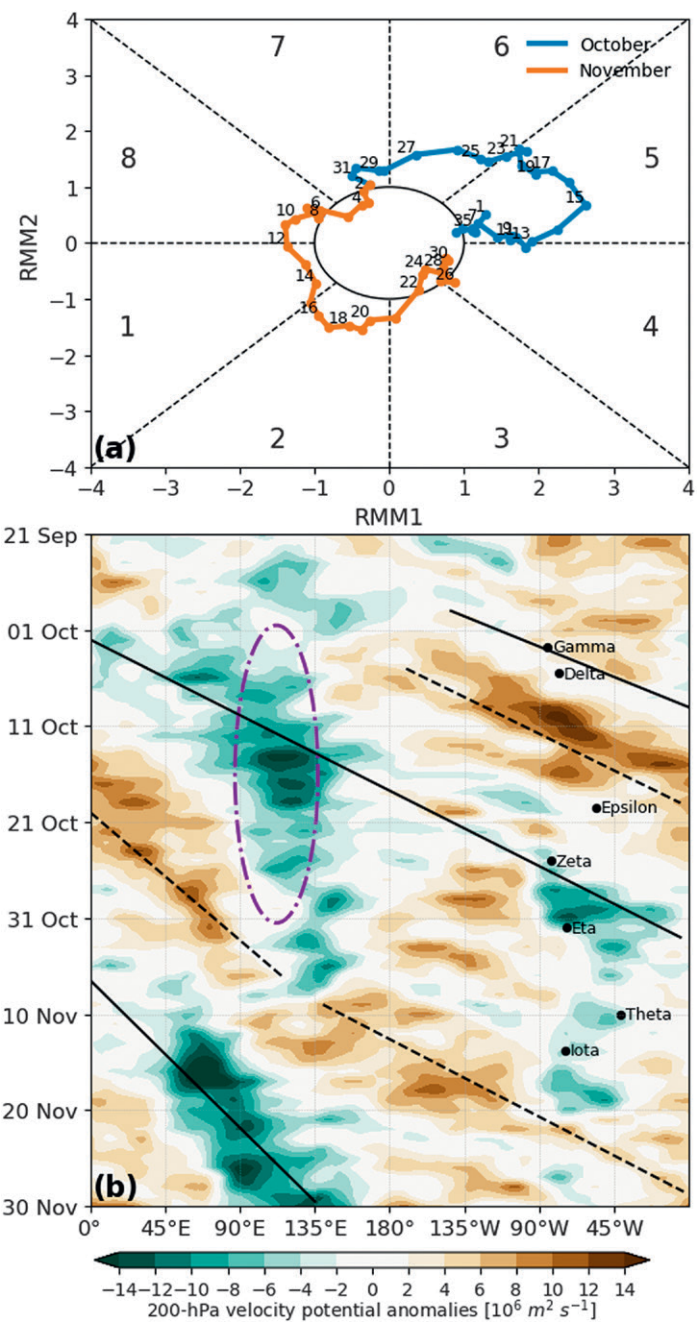


Fig. 8. (a) Propagation of the Madden–Julian oscillation during October–November 2020 according to the Wheeler and Hendon (2004) index. (b) Hovmöller diagram of Oct–Nov 200-hPa velocity potential anomalies spanning the globe averaged over 5° S– 5° N. Convectively enhanced and convectively suppressed phases of the MJO are highlighted with solid and dashed lines, respectively. The relatively stationary enhancement of convection located around $\sim 120^{\circ}$ E is also highlighted with a dashed ellipse.

Oct–Nov Caribbean ACE as the average of the third and fourth highest observed ACE values from 1979 to 2019, since the value in 2020 was predicted to fall between these two quantities. The final ACE forecast for Oct–Nov Caribbean ACE in 2020 would have been $27 \times 10^4 \text{ kt}^2$, just below the observed value and well above the 1979–2019 climatological Oct–Nov Caribbean ACE of $6 \times 10^4 \text{ kt}^2$. Consequently, the active late season in the Caribbean would have been well forecasted using this model.

Summary.

October–November (Oct–Nov) 2020 produced an extremely active end to the Atlantic hurricane season, with seven named storms, six hurricanes, five major hurricanes, and $74 \times 10^4 \text{ kt}^2$ accumulated cyclone energy (ACE) generated during the 2-month period (Table 1). From 1950 to 2019, a total of five major Atlantic hurricanes formed in November. In November 2020 alone, two major hurricanes (Eta and Iota) formed. In addition to producing the most major hurricanes and the second-most ACE during the final two months of the Atlantic hurricane season since 1950, five named storms (Gamma, Delta, Zeta, Eta, and Iota) made a combined 10 landfalls in Central America, the Caribbean, and the United States. Three of these hurricanes made landfall on the Yucatan Peninsula (Gamma, Delta, and Zeta; Fig. 4a inset). One category 3 hurricane (Zeta), one category 2 hurricane (Delta), and one tropical storm (Eta) made landfall in the United States. The most impactful landfalls, however, were two category 4 hurricanes which made landfall in nearly the same location in Nicaragua just 13 days apart (Fig. 4a inset). Eta and Iota caused devastation in Nicaragua, Honduras, and other portions of Central America as well as part of southern Mexico.

In addition, six Oct–Nov named storms (Gamma, Delta, Epsilon, Zeta, Eta, and Iota) intensified by $\geq 30 \text{ kt}$ in 24 h or less—defined as rapid intensification in this study (Kaplan and DeMaria 2003). These six rapidly intensifying TCs are the most during Oct–Nov since 1950, breaking the old record

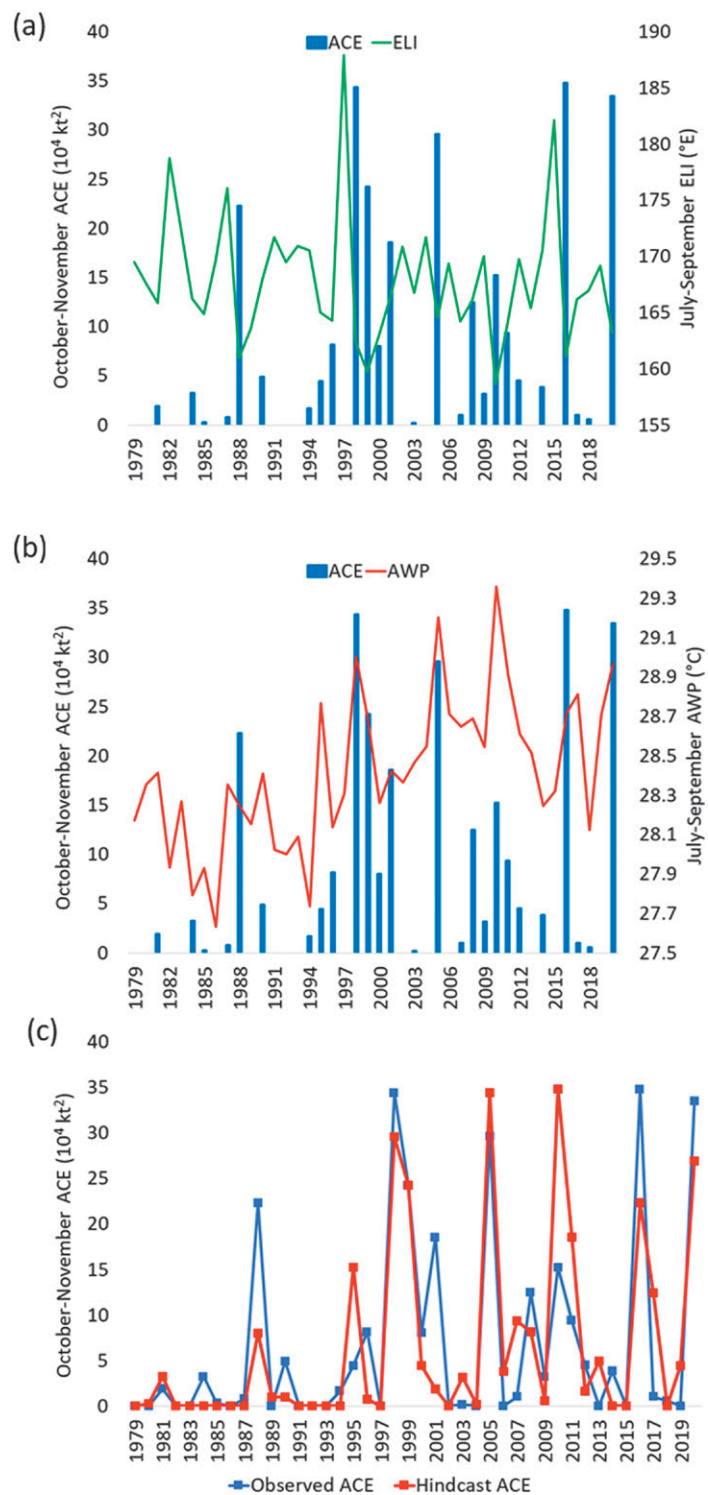


Fig. 9. (a) July–September ELI (green line) and October–November Caribbean ACE (blue columns) from 1979 to 2020. The correlation between the two time series from 1979 to 2019 is -0.54. (b) As in (a), but for July–September AWP (red line) and October–November Caribbean ACE (blue columns). The correlation between the two time series from 1979 to 2019 is 0.52. (c) October–November Caribbean ACE and hindcast ACE using July–September ELI and July–September AWP as predictors. The correlation between observed and hindcast ACE from 1979 to 2019 is 0.78.

How accurate is the Atlantic hurricane database?

The Atlantic hurricane database (HURDAT2; Landsea and Franklin 2013) extends back to 1851, providing a 170-yr record of TCs in the Atlantic basin. However, the TC records in this database are subject to a continuously improving observational network and, consequently, care must be used when examining long-term trends using this dataset. Here, we document several of the most notable observational improvements that have led to nonstationarity in TC records in the HURDAT2 dataset.

Though HURDAT2 began in 1851, the first notable observational improvement came in 1878 when the U.S. Signal Corps began consistently tracking hurricanes (Vecchi and Knutson 2008). This improvement is noted in simple counts of Atlantic hurricanes, with only one season from 1851 to 1877 recording more than seven hurricanes. For reference, the 1991–2020 Atlantic hurricane season average was seven hurricanes. These storms were also tracked farther east in the Atlantic beginning in 1878, allowing for larger ACE values to be generated by individual storms. For example, the largest ACE value in HURDAT2 from 1851 to 1877 was $88.4 \times 10^4 \text{ kt}^2$ in 1871, while from 1878 to 1899, 12 years had ACE values exceeding $100 \times 10^4 \text{ kt}^2$.

The continental United States landfalling hurricane record does extend back to 1851, but the record is likely incomplete prior to 1900 when the entire U.S. coastline from Texas to Maine was sufficiently populated to accurately record hurricane landfall intensities. Prior to ~1900, when hurricanes made landfall in sparsely populated portions of the coastline, they may have been incorrectly classified as tropical storms at landfall (Landsea 2015).

Another notable improvement in Atlantic hurricane observations came with the initiation of routine aircraft reconnaissance in 1944 (Hagen et al. 2012) following the pioneering flight of Joseph Duckworth and Ralph O'Hair into a 1943 hurricane in the Gulf of Mexico. Aircraft reconnaissance enabled

more accurate estimates of storm intensities, especially in the western Atlantic when storms were threatening land. Aircraft would also fly east from the Lesser Antilles to assess developing tropical depressions and tropical storms. Reconnaissance of Atlantic TCs has become more frequent in the past few decades, and the techniques used by aircraft to observe TCs have become much more sophisticated, now including the use of Global Positioning System (GPS) dropsondes and the Stepped Frequency Microwave Radiometer to assess surface wind speed.

The advent of polar-orbiting satellites in the mid-1960s provided one of the most significant improvements in Atlantic hurricane observations. These satellites observed Atlantic TCs multiple times per day, and this frequency further improved with geostationary satellite imagery beginning in the mid-1970s. The development of the Dvorak technique (Dvorak 1975) supported consistent interpretation of TC intensity from satellite imagery. Consequently, since the early to mid-1970s, Atlantic hurricane counts and ACE are likely mostly reliable.

Since ~2000, the availability of scatterometer winds and the cyclone phase space diagram has helped forecasters identify weaker TCs that may have gone undetected earlier in the Atlantic TC record. These developments have led to a nonphysical increase in short-lived named storms (e.g., named storms lasting two days or less), as noted by Landsea et al. (2010) and more recently by Schreck et al. (2021). On average, ~2 short-lived storms per year are named with today's technology than likely would have been named prior to ~2000. All of these technological developments, as well as others noted in Fig. SB1, should be accounted for when examining TC trends using HURDAT2 and associated Atlantic hurricane datasets.

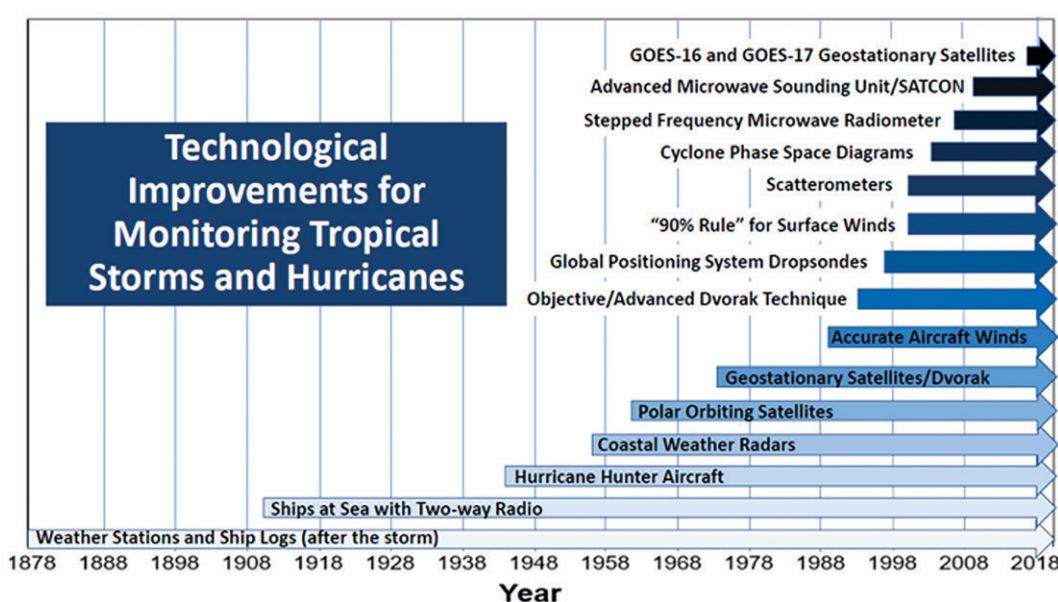


Fig. SB1. Major technological improvements since the start of the Atlantic hurricane database (HURDAT2) in 1851. Figure courtesy of Chris Landsea.

of three (set in 2005 and tied in 2010). Also, three named storms intensified by ≥ 65 kt in 24 h (Delta, Eta, and Iota). Only one named storm on record in Oct–Nov had intensified at such a rate prior to 2020 (Wilma in 2005, which intensified by 95 kt in 24 h).

Environmental conditions were more favorable than average in October in the western Atlantic including the Gulf of Mexico and Caribbean and were extremely favorable in November in the western Caribbean. October vertical wind shear, SST, and potential intensity all ranked in the 10 most favorable years since 1979 in both the western Caribbean and Gulf of Mexico. In November, large-scale conditions were extremely favorable in the western Caribbean and less favorable elsewhere. Vertical wind shear, midlevel humidity, and potential intensity in the western Caribbean were at or near their most favorable November values on record. When compared with the very active late western Caribbean TC season of 2005, large-scale environmental conditions were generally more conducive in the western Caribbean in October 2020 than they were in October 2005, and environmental conditions were much more conducive in November 2020 than they were in November 2005. The MJO likely enhanced convection and suppressed vertical wind shear over the western Caribbean from late October through mid-November of 2020, assisting in the intensification of Eta and Iota.

The extremely active late season in the Caribbean would have been well anticipated by a two-predictor model using the July–September–averaged ENSO longitude index and Atlantic warm pool SSTs as predictors. This two-predictor model explained $\sim 60\%$ of Oct–Nov Caribbean ACE variability from 1979 to 2019 and would have predicted an Oct–Nov Caribbean ACE of 27×10^4 kt 2 in 2020, just below the 33×10^4 kt 2 that was observed and well above the 1979–2019 average of 6×10^4 kt 2 . Colorado State University intends to begin issuing Oct–Nov Caribbean TC forecasts using this two-predictor model in 2021.

Acknowledgments. We would like to acknowledge the three anonymous reviewers and the editor, Chris Landsea, for helpful comments that significantly improved the manuscript. P. Klotzbach thanks the G. Unger Vetlesen Foundation for financial support that helped fund this research. K. Wood was supported by National Science Foundation Award AGS-2011812. M. Bell was supported by Office of Naval Research Award N000141613033. E. Gibney's research was supported by NOAA's Science Collaboration Program and administered by UCAR's Cooperative Programs for the Advancement of Earth System Science (CPAESS) under Awards NA16NWS4620043 and NA18NWS4620043B. C. Schreck was supported by NOAA through the Cooperative Institute for Satellite Earth System Studies under Cooperative Agreement NA19NES4320002. We thank Christina Patricola for providing the ENSO longitude index and Chris Landsea for providing Fig. SB1.

Data availability statement. All of the data used in this study are publicly available at the following URLs: continental U.S. hurricane landfalls (www.aoml.noaa.gov/hrd/hurdat/UShurrs_detailed.html), EM-DAT (<https://public.emdat.be>), ENSO longitude index (<https://portal.nersc.gov/archive/home/projects/cascade/www/ELI>), ERA5 (<https://cds.climate.copernicus.eu/#!/search?text=ERA5&type=dataset>), HURDAT2 (www.aoml.noaa.gov/hrd/hurdat/hurdat2.html), oceanic Niño index (https://origin.cpc.ncep.noaa.gov/products/analysis_monitoring/ensostuff/ONI_v5.php), and the Wheeler–Hendon MJO index (www.bom.gov.au/climate/mjo/graphics/rmm.74toRealtime.txt).

References

- Aon, 2021: Weather, Climate and Catastrophe insight: 2020 Annual Report. Aon, 81 pp., <http://thoughtleadership.aon.com/Documents/20210125-if-annual-cat-report.pdf>.
- Barnston, A. G., M. Chelliah, and S. B. Goldenberg, 1997: Documentation of a highly ENSO-related SST region in the equatorial Pacific: Research note. *Atmos.–Ocean*, **35**, 367–383, <https://doi.org/10.1080/07055900.1997.9649597>.
- Bell, G. D., and Coauthors, 2000: Climate assessment for 1999. *Bull. Amer. Meteor. Soc.*, **81**, 1328, [https://doi.org/10.1175/1520-0477\(2000\)081<1328:CAF>2.0.CO;2](https://doi.org/10.1175/1520-0477(2000)081<1328:CAF>2.0.CO;2).
- Beven, J. L., 2002: Tropical Cyclone Report: Hurricane Michelle. National Hurricane Center, 20 pp., www.nhc.noaa.gov/data/tcr/AL152001_Michelle.pdf.
- , 2021: Tropical Cyclone Report: Tropical Storm Theta. National Hurricane Center, 15 pp., www.nhc.noaa.gov/data/tcr/AL302020_Theta.pdf.
- , and Coauthors, 2008: Atlantic hurricane season of 2005. *Mon. Wea. Rev.*, **136**, 1109–1173, <https://doi.org/10.1175/2007MWR2074.1>.
- Bister, M., and K. A. Emanuel, 2002: Low frequency variability of tropical cyclone potential intensity: 1. Interannual to interdecadal variability. *J. Geophys. Res.*, **107**, 4801, <https://doi.org/10.1029/2001JD000776>.
- Blake, E. S., R. Berg, and A. Hagen, 2021: Tropical Cyclone Report: Hurricane Zeta. National Hurricane Center, 56 pp., www.nhc.noaa.gov/data/tcr/AL282020_Zeta.pdf.
- Brennan, M. J., 2009: Tropical Cyclone Report: Hurricane Paloma. National Hurricane Center, 21 pp., www.nhc.noaa.gov/data/tcr/AL172008_Paloma.pdf.
- Brown, D. P., 2017: Tropical Cyclone Report: Hurricane Otto. National Hurricane Center, 28 pp., www.nhc.noaa.gov/data/tcr/AL162016_Otto.pdf.
- Cangialosi, J. P., and R. Berg, 2021: Tropical Cyclone Report: Hurricane Delta. National Hurricane Center, 46 pp., www.nhc.noaa.gov/data/tcr/AL262020_Delta.pdf.
- Case, R. A., 1985: Tropical Cyclone Report: Hurricane Kate. National Hurricane Center, 16 pp., www.nhc.noaa.gov/archive/storm_wallets/atlantic/atl1985-prelim/kate/.
- Dawson, A., 2016: Windspharm: A high-level library for global wind field computations using spherical harmonics. *J. Open Res. Software*, **4**, e31, <https://doi.org/10.5334/jors.129>.
- DeMaria, M., J. A. Knaff, and B. H. Connell, 2001: A tropical cyclone genesis parameter for the tropical Atlantic. *Wea. Forecasting*, **16**, 219–233, [https://doi.org/10.1175/1520-0434\(2001\)016<0219:ATCGPF>2.0.CO;2](https://doi.org/10.1175/1520-0434(2001)016<0219:ATCGPF>2.0.CO;2).
- Dvorak, V. F., 1975: Tropical cyclone intensity analysis and forecasting from satellite imagery. *Mon. Wea. Rev.*, **103**, 420–430, [https://doi.org/10.1175/1520-0493\(1975\)103<0420:TCIAAF>2.0.CO;2](https://doi.org/10.1175/1520-0493(1975)103<0420:TCIAAF>2.0.CO;2).
- Efron, B., 1979: Bootstrap methods: Another look at the jackknife. *Ann. Stat.*, **7**, 1–26, <https://doi.org/10.1214/aos/1176344552>.
- Elsner, J. B., G. S. Lehmler, and T. B. Kimberlain, 1996: Objective classification of Atlantic hurricanes. *J. Climate*, **9**, 2880–2889, [https://doi.org/10.1175/1520-0442\(1996\)009<2880:OCOAH>2.0.CO;2](https://doi.org/10.1175/1520-0442(1996)009<2880:OCOAH>2.0.CO;2).
- EM-DAT, 2021: The International Disaster Database. Accessed 27 January 2021, <https://public.emdat.be>.
- Gilford, D. M., 2020: pyPI (v1.3): Tropical cyclone potential intensity calculations in Python. *Geosci. Model Dev.*, **14**, 2351–2369, <https://doi.org/10.5194/gmd-14-2351-2021>.
- Goldenberg, S. B., C. W. Landsea, A. M. Mestas-Nuñez, and W. M. Gray, 2001: The recent increase in Atlantic hurricane activity: Causes and implications. *Science*, **293**, 474–479, <https://doi.org/10.1126/science.1060040>.
- Gray, W. M., 1984: Atlantic seasonal hurricane frequency. Part I: El Niño and 30 mb quasi-biennial oscillation influences. *Mon. Wea. Rev.*, **112**, 1649–1668, [https://doi.org/10.1175/1520-0493\(1984\)112<1649:ASHFPI>2.0.CO;2](https://doi.org/10.1175/1520-0493(1984)112<1649:ASHFPI>2.0.CO;2).
- Guiney, J. L., 1999: Tropical Cyclone Report: Hurricane Lenny. National Hurricane Center, 19 pp., www.nhc.noaa.gov/data/tcr/AL161999_Lenny.pdf.
- Hagen, A. B., D. Strahan-Sakoskie, and C. Luckett, 2012: A reanalysis of the 1944–53 Atlantic hurricane seasons—The first decade of aircraft reconnaissance. *J. Climate*, **25**, 4441–4460, <https://doi.org/10.1175/JCLI-D-11-00419.1>.
- Hersbach, H., and Coauthors, 2020: The ERA5 global reanalysis. *Quart. J. Roy. Meteor. Soc.*, **146**, 1999–2049, <https://doi.org/10.1002/qj.3803>.
- Hesterberg, T., S. Monaghan, D. S. Moore, A. Clipson, and R. Epstein, 2003: *Bootstrap Methods and Permutation Tests: Companion Chapter 18 to The Practice of Business Statistics*. W. H. Freeman and Company, 85 pp., <https://statweb.stanford.edu/~tibs/stat315a/Supplements/bootstrap.pdf>.
- Johnson, N. C., and S.-P. Xie, 2010: Changes in the sea surface temperature threshold for tropical convection. *Nat. Geosci.*, **3**, 842–845, <https://doi.org/10.1038/ngeo1008>.
- Kaplan, J., and M. DeMaria, 2003: Large-scale characteristics of rapidly intensifying tropical cyclones in the North Atlantic basin. *Wea. Forecasting*, **18**, 1093–1108, [https://doi.org/10.1175/1520-0434\(2003\)018<1093:LCORIT>2.0.CO;2](https://doi.org/10.1175/1520-0434(2003)018<1093:LCORIT>2.0.CO;2).
- , —, and J. A. Knaff, 2010: A revised tropical cyclone rapid intensification index for the Atlantic and eastern North Pacific basins. *Wea. Forecasting*, **25**, 220–241, <https://doi.org/10.1175/2009WAF2222280.1>.
- Klotzbach, P. J., 2007: Revised prediction of seasonal Atlantic basin tropical cyclone activity from 1 August. *Wea. Forecasting*, **22**, 937–949, <https://doi.org/10.1175/WAF1045.1>.
- , 2010: On the Madden–Julian oscillation–Atlantic hurricane relationship. *J. Climate*, **23**, 282–293, <https://doi.org/10.1175/2009JCLI2978.1>.
- , 2011: Forecasting October–November Caribbean hurricane days. *J. Geophys. Res.*, **116**, D18117, <https://doi.org/10.1029/2011JD016146>.
- , and W. M. Gray, 2008: Multi-decadal variability in North Atlantic tropical cyclone activity. *J. Climate*, **21**, 3929–3935, <https://doi.org/10.1175/2008JCLI2162.1>.
- , and C. W. Landsea, 2015: Extremely intense hurricanes: Revisiting Webster et al. (2005) after 10 years. *J. Climate*, **28**, 7621–7629, <https://doi.org/10.1175/JCLI-D-15-0188.1>.
- , and E. C. J. Oliver, 2015: Modulation of Atlantic basin tropical cyclone activity by the Madden–Julian Oscillation (MJO) from 1905–2011. *J. Climate*, **28**, 204–217, <https://doi.org/10.1175/JCLI-D-14-00509.1>.
- , S. G. Bowen, R. Pielke Jr., and M. M. Bell, 2018: Continental United States landfall frequency and associated damage: Observations and future risks. *Bull. Amer. Meteor. Soc.*, **99**, 1359–1376, <https://doi.org/10.1175/BAMS-D-17-0184.1>.
- , M. M. Bell, and J. Jones, 2020: Forecast of Atlantic seasonal hurricane activity and landfall strike probability for 2020. Dept. of Atmospheric Science Rep., Colorado State University, Fort Collins, CO, 31 pp., <https://tropical.colostate.edu/Forecast/2020-08.pdf>.
- Landsea, C. W., 2007: Counting Atlantic tropical cyclones back to 1900. *Eos, Trans. Amer. Geophys. Union*, **88**, 197–202, <https://doi.org/10.1029/2007EO180001>.
- , 2015: Comments on “Monitoring and understanding trends in extreme storms: State of knowledge.” *Bull. Amer. Meteor. Soc.*, **96**, 1175–1176, <https://doi.org/10.1175/BAMS-D-13-00211.1>.
- , and J. L. Franklin, 2013: Atlantic hurricane database uncertainty and presentation of a new database format. *Mon. Wea. Rev.*, **141**, 3576–3592, <https://doi.org/10.1175/MWR-D-12-00254.1>.
- , G. A. Vecchi, L. Bengtsson, and T. R. Knutson, 2010: Impact of duration thresholds on Atlantic tropical cyclone counts. *J. Climate*, **23**, 2508–2519, <https://doi.org/10.1175/2009JCLI3034.1>.
- Latto, A. S., 2021: Tropical Cyclone Report: Hurricane Gamma. National Hurricane Center, 20 pp., www.nhc.noaa.gov/data/tcr/AL252020_Gamma.pdf.
- Madden, R. A., and P. R. Julian, 1971: Detection of a 40–50 day oscillation in the zonal wind in the tropical Pacific. *J. Atmos. Sci.*, **28**, 702–708, [https://doi.org/10.1175/1520-0469\(1971\)028<0702:DOADOI>2.0.CO;2](https://doi.org/10.1175/1520-0469(1971)028<0702:DOADOI>2.0.CO;2).
- McTaggart-Cowan, R., T. J. Galarneau, L. F. Bosart, R. W. Moore, and O. Martius, 2013: A global climatology of baroclinically influenced tropical cyclogenesis. *Mon. Wea. Rev.*, **141**, 1963–1989, <https://doi.org/10.1175/MWR-D-12-00186.1>.
- Papin, P. P., 2021: Tropical Cyclone Report: Hurricane Epsilon. National Hurricane Center, 23 pp., www.nhc.noaa.gov/data/tcr/AL272020_Epsilon.pdf.
- , L. F. Bosart, and R. D. Torn, 2017: A climatology of Central American gyres. *Mon. Wea. Rev.*, **145**, 1983–2000, <https://doi.org/10.1175/MWR-D-16-0411.1>.

- Pasch, R. J., and D. P. Roberts, 2006: Tropical Cyclone Report: Hurricane Stan. National Hurricane Center, 12 pp., www.nhc.noaa.gov/data/tcr/AL202005_Stan.pdf.
- , L.A. Avila, and J.L. Guiney, 2001: Atlantic hurricane season of 1998. *Mon. Wea. Rev.*, **129**, 3085–3123, [https://doi.org/10.1175/1520-0493\(2001\)129<3085:AHSO>2.0.CO;2](https://doi.org/10.1175/1520-0493(2001)129<3085:AHSO>2.0.CO;2).
- , B. J. Reinhardt, R. Berg, and D. P. Roberts, 2021: Tropical Cyclone Report: Hurricane Eta. National Hurricane Center, 70 pp., www.nhc.noaa.gov/data/tcr/AL292020_Eta.pdf.
- Roundy, P. E., 2012: Observed structure of convectively coupled waves as a function of equivalent depth: Kelvin waves and the Madden–Julian oscillation. *J. Atmos. Sci.*, **69**, 2097–2106, <https://doi.org/10.1175/JAS-D-12-03.1>.
- Schreck, C. J., P. J. Klotzbach and M. M. Bell, 2021: Optimal climate normals for North Atlantic hurricane activity. *Geophys. Res. Lett.*, **48**, e2021GL092864, <https://doi.org/10.1029/2021GL092864>.
- Smith, W. L., H. M. Woolf, C. M. Hayden, D. Q. Wark, and L. M. McMillin, 1979: The TIROS-N operational vertical sounder. *Bull. Amer. Meteor. Soc.*, **60**, 1177–1187, <https://doi.org/10.1175/1520-0477-60.10.1177>.
- Stewart, S. R., 2021: Tropical Cyclone Report: Hurricane Iota. National Hurricane Center, 49 pp., www.nhc.noaa.gov/data/tcr/AL312020_Iota.pdf.
- Tang, B. H., and J. D. Neelin, 2004: ENSO influence on Atlantic hurricanes via tropospheric warming. *Geophys. Res. Lett.*, **31**, L24204, <https://doi.org/10.1029/2004GL021072>.
- , and Coauthors, 2020: Recent advances in research on tropical cyclogenesis. *Trop. Cyclone Res. Rev.*, **9**, 87–105, <https://doi.org/10.1016/j.tctr.2020.04.004>.
- Vecchi, G. A., and T. R. Knutson, 2008: On estimates of historical North Atlantic tropical cyclone activity. *J. Climate*, **21**, 3580–3600, <https://doi.org/10.1175/2008JCLI2178.1>.
- Ventrice, M. J., C. D. Thorncroft, and P. E. Roundy, 2011: The Madden–Julian oscillation’s influence on African easterly waves and downstream tropical cyclogenesis. *Mon. Wea. Rev.*, **139**, 2704–2722, <https://doi.org/10.1175/MWR-D-10-05028.1>.
- Wang, C., and S.-K. Lee, 2007: Atlantic warm pool, Caribbean low-level jet and their potential impact on Atlantic hurricanes. *Geophys. Res. Lett.*, **34**, L02703, <https://doi.org/10.1029/2006GL028579>.
- Wheeler, M. C., and H. H. Hendon, 2004: An all-season real-time multivariate MJO index: Development of an index for monitoring and prediction. *Mon. Wea. Rev.*, **132**, 1917–1932, [https://doi.org/10.1175/1520-0493\(2004\)132<1917:AARM>2.0.CO;2](https://doi.org/10.1175/1520-0493(2004)132<1917:AARM>2.0.CO;2).
- Wilks, D. S., 1997: Resampling hypothesis tests for autocorrelated fields. *J. Climate*, **10**, 65–82, [https://doi.org/10.1175/1520-0442\(1997\)010<0065:RHTFA>2.0.CO;2](https://doi.org/10.1175/1520-0442(1997)010<0065:RHTFA>2.0.CO;2).
- Williams, I. N., and C. M. Patricola, 2018: Diversity of ENSO events unified by convective threshold sea surface temperature: A nonlinear ENSO index. *Geophys. Res. Lett.*, **45**, 9236–9244, <https://doi.org/10.1029/2018GL079203>.